ELSEVIER

Journal of Nuclear Materials 313–316 (2003) 925–930

journal of nuclear materials

www.elsevier.com/locate/jnucmat

Tomographic reconstruction of 2D line radiation distribution in the JET MkIIGB divertor

A. Huber [a,*], P. Coad [b], D. Coster [c], L.C. Ingesson [d], K. Itami [e], S. Jachmich [a], A. Kirschner [a], M. Lehnen [a], G.F. Matthews [b], Ph. Mertens [a], V. Philipps [a], A. Pospieszczyk [a], B. Schweer [a], G. Sergienko [f], M. Stamp [b], Contributors to the EFDA-JET programme

[a] *Institut für Plasmaphysik, Forschungszentrum Jülich GmbH, EURATOM Association, Trilateral Euregio Cluster (TEC), D-52425 Jülich, Germany*

[b] *Euratom/UKAEA Fusion Association, Culham Science Centre, Abingdon, Oxon OX14 3DB, UK*

[c] *Max-Planck-Institut für Plasmaphysik, D-85748 Garching, Germany*

[d] *FOM-Instituut voor Plasmafysica, P.O. Box 1207, 3430 BE Nieuwegein, The Netherlands*

[e] *Japan Atomic Energy Research Institute, Naka-machi, Ibaraki-ken 311-0193, Japan*

[f] *Institute of High Temperatures, Russian Academy of Sciences, 127412 Moscow, Russian Federation*

Received 27 May 2002; accepted 26 September 2002

Abstract

A 2D-tomographic reconstruction of D_α- and C III-emission distribution in L-mode, density limit discharge has been performed and compared with results from other diagnostics (KL2, KS3). The observed emission patterns in a poloidal plane show a strong in–out asymmetry, which depends on local plasma parameter in the divertor. It is shown that the major contribution to D_α-emission, under the observed conditions, lies in excitation processes and that low-energy charge-exchange reactions with neutral deuterium can influence the ionisation balance of carbon and the recorded C III-emission line. The evolution of the intrinsic hydrogen and carbon impurity profiles has been analysed with respect to its dependence on the location of methane fuelling.

PACS: 52.40.H

1. Introduction

The amount and spatial distribution of impurity radiation in the divertor of a tokamak is of fundamental importance for the behaviour of power exhaust, detachment, recombination, recycling and erosion/redeposition properties. Carbon impurity radiation in the divertor is desirable to reduce the peak heat flux to the strike zones. But carbon erosion contributes also to MARFE formation, limits the lifetime of the target and leads to large tritium retention via co-deposition. In addition to line-integrated spectroscopic measurements, the recording of spatially resolved radiation of the various species obtained from tomographic inversion of 2D-CCD camera data is an important tool for diagnosing the role of impurity and hydrogen radiation in the divertor physics.

2. Experimental setup

At JET, three CCD cameras (KL1 diagnostic system, dynamical range of 8 bits, CCD-chip with

* Corresponding author: Tel.: +49-2461 61 2631; fax: +49-2461 61 2660.

E-mail address: a.huber@fz-juelich.de (A. Huber).

0022-3115/03/$ - see front matter
PII: S0022-3115(02)01478-2

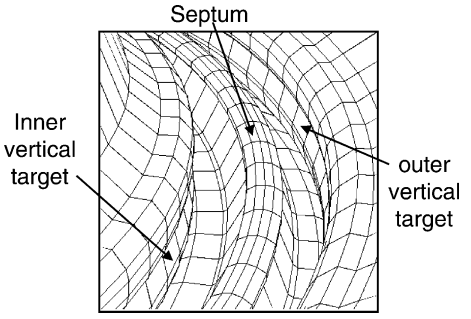

Fig. 1. View of CCD cameras into the divertor.

582 × 752 pixels) view the divertor in a nearly tangential geometry, as shown in Fig. 1. They are coupled with interference filters and allow measurements of line-emission at three wavelengths (e.g. D_α, C II and C III simultaneously). Video signals are captured with a frame-grabber board, which transfers all images directly into the main memory. These cameras take video pictures at 50 half-frames per second. The evaluation of the 2D-emission distribution in a poloidal plane assumes toroidal symmetry and is obtained by solving the matrix equation $\boldsymbol{Ax} = \boldsymbol{b}$ using the singular value decomposition method [1]. Here, $\boldsymbol{A}$ is the 'geometry matrix' that contains the information on the geometric view of each CCD-pixel and on the divertor structures limiting the corresponding lines of sight. The vector $\boldsymbol{b}$ contains the raw data (digitised CCD data). The poloidal distribution $\boldsymbol{x}$ is the unknown. The CCD camera tomography system similar to the JET system was at first successfully applied on DIII-D tokamak [2,3], and is in the meantime improved [4] for fast measurements with time resolution below the duration of an edge localised mode. As shown in Ref. [5], the camera system at JET has enough chords in the whole divertor region to resolve the emission patterns along the radial direction with sufficient resolution (<0.2 cm), but the resolution in z-direction (i.e. vertically, see Fig. 3) is limited to about 5 cm, owing to the small number of chords that actually cross each other at large angles.

The D_α distribution across inner and outer divertor is obtained with a spatial resolution of 3 mm from the vertical view of an additional linear camera (KL2). A survey spectrometer in the visible (KS3) provides integrated D_α- and C III-signals over both divertor legs. These two diagnostics are used for cross-calibration and for comparison with the reconstructed 2D distributions of the line radiation.

3. Results and discussion

L-mode 'density limit' experiments have been performed with $B_T = 2.4$ T, $I_p = 2$ MA and with an additional NBI power of 2.3 MW. Fig. 2 shows the time evolution of a typical L-mode density limit discharge in JET with the MkIIGB divertor. The plasma density was raised steadily to the density limit ($n_e^{max} = 4.5 \times 10^{19}$ m^{-3} at $t = 60.3$ s) by gas fuelling at constant input power. The integral ion flux to the outer divertor, measured by an array of Langmuir probes, initially increases, while the flux to the inner divertor remains low with continuously decrease until the discharge disruption. This indicates that the inner divertor is partially detached from the start. But D_α-emission in the inner divertor (see Fig. 4) and neutral pressure in the divertor chamber (not shown) continue to increase. This is the signature of plasma detachment [6], which is characterised by a substantial drop both in particle and energy fluxes to the target plates, as well as in the pressure along the magnetic field lines. Shortly before the discharge disrupts, the ion flux to the outer divertor drops dramatically: a MARFE forms, which leads to a 'density limit' disruption. During the time of the density increase, the total radiated power is always increasing, too. The temporal behaviour of the ratio D_γ/D_α will be discussed later on.

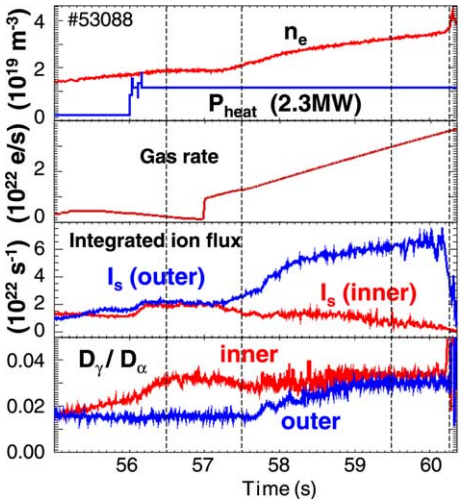

Fig. 2. Time evolution of a typical L-mode, density limit discharge in JET with the MkIIGB divertor. The figure shows the central averaged density, the NBI input power, the integrated ion flux to inner and outer divertors and D_γ/D_α-emission line ratios at the inner and outer targets. The line averaged central density reached a value of 4.5×10^{19} m^{-3} at $t = 60.3$ s when the disruption occurs (so called the 'maximum density'). The vertical dashed lines indicate the times at which the tomographic reconstructions of observed emission lines are presented in Fig. 3.

Fig. 3 shows the tomographic reconstruction of D_α- (top) and C III-emission (bottom) in the divertor region at four different points in time:

Time 56.5 s: In this early phase of the discharge, the maximum of the hydrogen radiation is located near

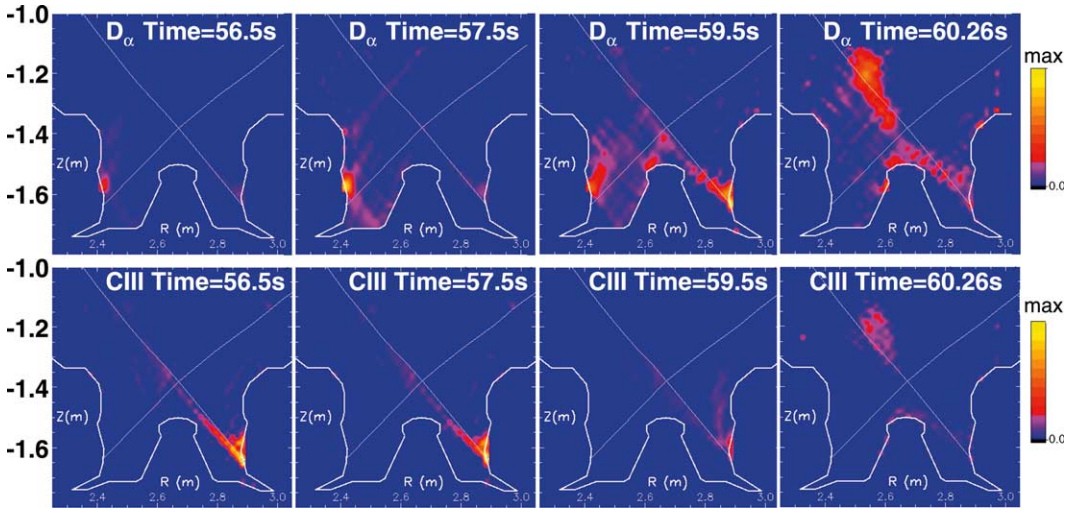

Fig. 3. Tomographic reconstruction of D_α- (top) and C III-emission (bottom) in the divertor region measured by tangential CCD cameras during four phases of the L-mode density limit discharge (same shot as shown in Fig. 2).

the target plates at the position of the strike zone but with significantly more radiation from the inner leg than from the outer. The electron temperature near the inner and outer strike points is about 8 and 18 eV, respectively. The C III-radiation is much stronger in the outer divertor, with an additional significant contribution near the X-point.

Time 57.5 s: The D_α-emission rapidly increases in the inner divertor. The ion flux to the inner divertor decreases, which indicates the start of the detachment. The Langmuir probes measure values of $T_e \approx 3$–4 eV and $n_e = 2 \times 10^{19}$ m^{-3}, which, however, overestimates T_e, since the standard interpretation of the *I–V* characteristic does not apply in this regime [7]. A small decrease (about 20%) in the C III-emission is observed in the outer divertor leg ($T_e \approx 13$ eV).

Time 59.5 s: While the D_α-emission extends in two dimensions in the inner divertor, it increases linearly (see Fig. 4) with central average electron density along the outer leg (near the outer strike point, $T_e \approx 6$–7 eV). The spatial distribution of hydrogen radiation is, in this discharge phase, nearly symmetrical. The ion flux at the outer strike point also increases. A strong reduction of C III-emission in the outer leg is observed.

Time 60.26 s: A drastic change in the D_α-emission happens together with full detachment of the inner divertor. The emission takes off from the inner target and moves to the X-point. The C III-emission is positioned above the X-point, a MARFE forms and moves towards the inner wall, which leads to a density-limit disruption.

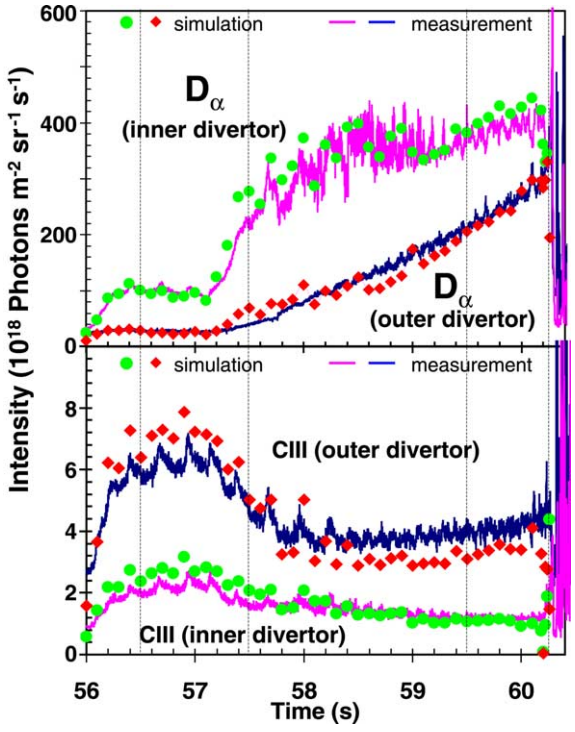

Fig. 4. Time evolution of D_α (top)- and C III (bottom)-line-integrated emissions, shown with simulated data from a tomographic reconstruction. The vertical dashed lines indicate the times at which the tomographic reconstructions of observed emission lines are presented in Fig. 3.

The KS3 visible survey spectrometer provides integrated D_α- and C III-signals over inner and outer

divertors, that are used for cross-calibration and for comparison with reconstructed 2D distributions of line radiation. Fig. 4 shows the time evolution of D_α (top)- and C III (bottom)-integrated emission both in inner and outer divertor. The solid lines show the data from the spectrometer, and the symbols correspond to the simulation from tomographic reconstruction. For this simulation, D_α- and C III-reconstructed emissions were integrated along the same chord and averaged over the same radial extent as of the spectrometer. One sees that the simulated integrated emissions match the measured ones well during the whole discharge (deviation are lower than 10% for D_α and 20% for C III, respectively).

The reconstructed D_α-emission profiles have also been compared with the line-integrated emission of the D_α hydrogen line, measured vertically from the top of the machine by an absolutely calibrated linear CCD camera (KL2). As can be seen in Fig. 5, the comparison between the reconstructed and the measured poloidal D_α-emission profiles for two different times shows a good agreement. These profiles show results similar to those presented in Fig. 3. At $t = 56.5$ s, the profile shows a strong in–out asymmetry with significantly more radiation from the inner leg. As the density increases, the hydrogen emission increases in both inner and outer divertors. An increase of intensity above the divertor septum is observed, too.

As shown above, the D_α- and C III-emissions show a definite in–out asymmetry, depending on local plasma parameters. Next we have to discuss how this asymmetry can be explained. As T_e at the inner strike point drops from 8 eV to values below 3–4 eV, D_α increases by a factor of 3.5–4.0. The lower value of T_e might be overestimated as mentioned above. However, from our spectroscopic observations we can deduce a lower limit of 1.5 eV as will be shown later. The ratio of ionisation per photon for D_α, the so-called S/XB-value, decreases by a factor of 2 (from 25 ($T_e = 8$ eV) to 12 ($T_e = 4$ eV)), thereby indicating an actual increase of a factor of 2 (and not a factor of 4) for the D_α-emission, due to excitation only. The increase of a factor 4 in the hydrogen emission – for excitation only – can be explained if the temperature drops to a value of about 2 eV. Fig. 6 shows the influence of recombination on hydrogen emission. Here, the D_α-emission rates corresponding to excitation ($\sim n_e n_0$, calculated for three different values of the neutral density n_0) and recombination ($\sim n_e^2$) for an electron density of $n_e = 2 \times 10^{19}$ m^{-3} are fetched from the ADAS data structure [8]. Thus, the ratio of the emission from recombination to excitation depends on the ratio n_e/n_0. With an increase of the ratio n_e/n_0 from 1 to 100, as shown in Fig. 6, the temperature, at which the ionisation

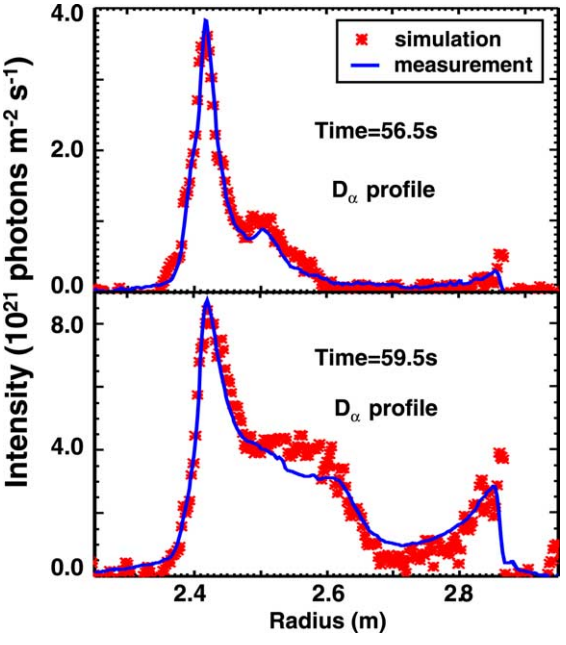

Fig. 5. Comparison of reconstructed and measured (KL2) D_α-emission profiles.

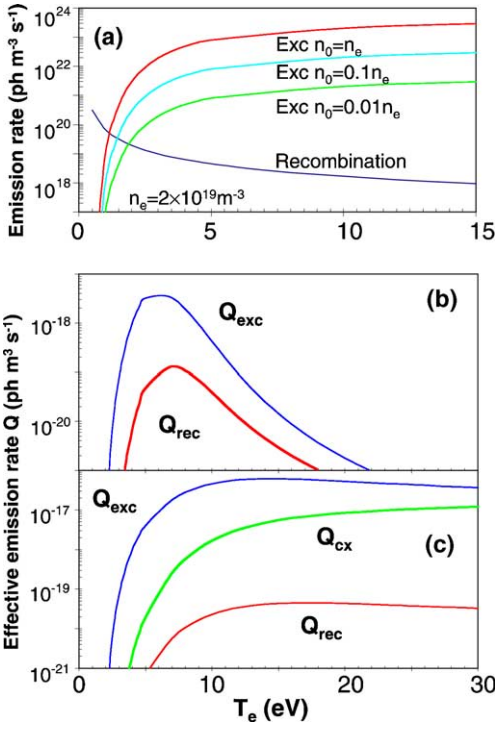

Fig. 6. (a) D_α-emission rates due to excitation (for three different neutral densities) and recombination for an electron density $n_e = 2 \times 10^{19}$ m^{-3} from ADAS [8]; (b) effective emission rates for excitation (Q_{exc}) and recombination (Q_{rec}); (c) effective emission rates Q_{exc}, Q_{rec} and Q_{cx} (charge exchange), taking into account the charge-exchange processes with neutral deuterium (at $n_e = 2 \times 10^{19}$ m^{-3} and a neutral density of $n_0 = 0.1 \times n_e$).

and recombination rates are equal, increases from 1 to 2 eV. One sees that the recombination becomes dominant for electron temperatures below 1.5 eV, for any reasonable neutral density. The influence of recombination on the ratio D_γ/D_α is discussed in detail in Ref. [9]. If it is assumed that the whole radiation is caused by recombination, the ratio D_γ/D_α must be between 0.15 and 0.2 for $n_e = 2 \times 10^{19}$ m^{-3} in the electronic temperature range $T_e = 0.5$–4.0 eV. If the whole radiation was due to excitation, the ratio D_γ/D_α would be below 0.018. The measured ratio at $t = 57.5$ s is about 0.03 (see Fig. 2), confirming that the major contributing process to the D_α-emission is excitation. Therefore, a lower limit of T_e is 1.5 eV.

Around 1.3 eV, the ionisation and recombination rate coefficients are approximately equal [10]. For this temperature, the recombination rate coefficient is relatively low ($\leqslant 10^{-17}$ m^3 s^{-1}), so that for $n_e = 2 \times 10^{19}$ m^{-3}, the characteristic time for recombination $\tau_{rec} \geqslant 5$ ms. It is comparable to or longer than the ion transit time in the divertor for a flow speed of $\sim 10^4$ m s^{-1}. There is thus no sufficient time for volume recombination to occur.

As shown above, the C III-radiation is much stronger in the outer divertor with the maximum at $T_e = 18$ eV. Fig. 6(b) shows effective emission rates for excitation Q_{exc} and recombination Q_{rec} for $n_e = 2 \times 10^{19}$ m^{-3} as function of the electron temperature. By 'effective emission rates' we mean the product of a photon emissivity coefficient (PEC) times the fractional abundance of carbon ions $f(^{Z+}) = n(C^{Z+})/n(C)$, where $n(C)$ and $n(C^{Z+})$ is the total carbon density and the density of carbon ions with atomic charge Z: $Q_{exc} = PEC_{exc} \times f(C^{2+})$, $Q_{rec} = PEC_{rec} \times f(C^{3+})$, $Q_{cx} = PEC_{cx} \times f(C^{3+})$, where Q_{cx} is an effective emission rate for charge exchange with neutral hydrogen. The volume photon emissivity of the observed line (C III, $\lambda = 465$ nm) can be written $\varepsilon = n_e \times n(C)[Q_{exc} + Q_{rec} + Q_{cx}]$. The PECs and fractional abundances were again calculated with the help of the ADAS structure and database. The maximum in the calculated intensity per C atom lies around 5 eV, whereas we observe a maximum at 18 eV. Therefore, ionisation and recombination processes alone cannot explain the observed C III-emission. Fig. 6(c) shows values of Q which take into account the charge exchange processes with neutral hydrogen (deuterium) at a density of $n_0 = 0.1 \times n_e$ (typical value calculated by means of B2–EIRENE code in the case of high-density JET divertor plasmas [11]). For $T_e = 18$ eV, the charge-exchange rate coefficient (C^{3+} with D) is relatively large ($\geqslant 2 \times 10^{-15}$ m^3 s^{-1}) [12], so that for $n_e = 2 \times 10^{19}$ m^{-3} = $10 \times n_0$, the characteristic time for charge-exchange $\tau_{cx} \leqslant 0.25$ ms, i.e. much smaller than the ion transit time in the divertor for a flow speed of $\sim 10^4$ m s^{-1}. Thus, charge-exchange processes can sufficiently influence the C III-emission.

The direct charge-exchange contribution Q_{cx} to the line emission is negligible compared to electron-impact excitation Q_{exc}. But it nevertheless shifts the ionisation balance to lower charge states (influence on $f(C^{2+})$ and correspondingly on Q_{exc}). The maximum of the calculated line emissivity per electron and carbon atom is shifted to higher electron temperatures at around 15 eV. This emissivity varies only weakly in the temperature range between 10 and 20 eV, showing a similar behaviour as in the experiment (Fig. 3 at $t = 56.5$ and 57.5 s). For small values of T_e, the line intensity drops sharply (it is more than one order of magnitude smaller for $T_e = 3$–4 eV, compared with $T_e = 15$ eV), as seen in the experimental data. For temperatures below 4 eV (for inner divertor at high density) the influence of charge exchange on C III-line emission is negligible (compare Q_{exc} in Fig. 6(b) and (c)) Thus, the strong in–out asymmetry in C III-emission can be explained by a strong in–out asymmetry in T_e with strong contribution of charge exchange in particular in the outer divertor. Another possible reason for asymmetrical C III-emission would be a strong asymmetry in carbon erosion fluxes in inner and outer legs: in the outer divertor, the physical sputtering of C due to the impact of D and C dominates, whereas in the inner divertor, the chemical erosion of carbon due to molecule formation can lead to strong erosion even for impact energies below the threshold for physical sputtering. In Ref. [13], spectroscopic clues for such a behaviour are discussed in detail for O II and the same line of C III as recorded in the present work. In order to study the influence of the impurity sources on line emission, a gas puffing experiment was performed. About 5×10^{21} CD_4 molecules per second were injected during L-mode discharges at different times into the inner and outer divertors, through a nozzle in the horizontal target plate (puff within the private flux zone). The magnetic configuration and plasma parameters were similar to the discharge shown in Fig. 2 at $t = 57.5$ s with strong in–out asymmetry: D_α radiates strongly in the inner leg, C III in the outer divertor. During the CD_4 injection into the outer divertor, the D_α-emission shows a small increase in the outer leg (about 30%), but it is still much smaller than the emission from the inner divertor (S/XB(D_α) at outer strike point is relatively large, about 25). C III-emission increases by about a factor of 2 in the vicinity of the gas puffing. The injection of CD_4 into the inner leg leads to a strong increase in D_α-emission (about a factor of 3–4), but to practically no change in the C III-emission in the inner divertor. Thus, the injection of the same amount of CD_4 into the inner and outer legs shows the different increase of D_α- and C III-emissions in these divertor regions. This indicates that the main reason for in–out divertor emission asymmetry is the asymmetry in the local electron temperature and not the difference of hydrogen and carbon sources. The behaviour of observed emissions during the

density increase can be explained by change of the local electron temperature.

4. Summary and conclusion

2D emission profiles of C III- and D_α-radiation in the JET divertor have been reconstructed by the singular value decomposition method to obtain the emission pattern in a poloidal plane. The reconstructed 2D distributions were compared with results from other diagnostics (KL2, KS3) and were in a good agreement.

Significant differences in line emission were observed between inner and outer divertor. At low central electron density ($\approx 2 \times 10^{19}$ m^{-3}), the maximum of the hydrogen radiation is located near the target plates at the position of the strike zone, but with significantly more radiation from the inner leg than from the outer. The C III-radiation is much stronger in the outer divertor, with a strong contribution near the X-point as well. With increasing density, D_α extends two-dimensionally within the inner divertor and, at the same time, it goes up in the outer divertor. The D_α-emission is, at that time, nearly symmetrical. During the density rise, a reduction in C III-emission is observed, which corresponds to a decrease of both the electron temperature and of the physical sputtering yield.

It has been shown that the major contributors to D_α-emission are, for the observed conditions, excitation processes and that low-energy charge-exchange reactions with neutral deuterium can influence the ionisation balance and the behaviour of the observed C III-emission line.

The evolution of the intrinsic hydrogen and carbon impurity profiles in L-mode discharges has been discussed, with respect to its dependence on the location of methane fuelling (inner/outer divertor leg). Interestingly, the C III-radiation of the carbon impurity fuelled via CD_4 injection in the divertor region shows a very similar pattern to that observed from intrinsic sources alone.

References

[1] G.H. Golub, C.F. Van Loan, Matrix Computations, John Hopkins University Press, Baltimore, 1983.
[2] M.E. Fenstermacher et al., Rev. Sci. Instrum. 68 (1) (1997) 974.
[3] M.E. Fenstermacher et al., J. Nucl. Mater. 266–269 (1999) 348.
[4] M. Groth et al., these Proceedings.
[5] A. Huber, P. Coad, D. Coster, et al., Proceedings of the 28th EPS Conference on Controlled Fusion and Plasma Physics, Funchal, ECA, vol. 25A, 2001, p. 1649.
[6] A. Loarte et al., Nucl. Fusion 38 (1998) 331.
[7] R.D. Monk et al., Contribution Plasma Phys. 36 (1996) 37.
[8] H.P. Summers, Atomic Data and Analysis Structure – User's Manual, Rep. IR(94) 06, JET Joint Undertaking, Abingdon, 1994. Available from <http://adas.phys.strath.ac.uk>.
[9] G.M. McCracken et al., Nucl. Fusion 38 (1998) 619.
[10] D.E. Post, J. Nucl. Mater. 220–222 (1995) 143.
[11] D. Reiser, private communication.
[12] C.F. Maggi et al., Plasma Phys. Control. Fusion 42 (2000) 669.
[13] J.D. Hey et al., J. Phys. B: At. Mol. Opt. Phys. 35 (2002) 1525.